PHYSICAL REVIEW B VOLUME 62, NUMBER 4 15 JULY 2000-II

Molecular-dynamics simulation of thermal stress at the (100) diamond/substrate interface: Effect of film continuity

Irina Rosenblum
Departments of Physics and Chemical Engineering, Technion-IIT, 32000, Haifa, Israel

Joan Adler*
Department of Physics, Technion-IIT, 32000, Haifa, Israel

Simon Brandon
Department of Chemical Engineering, Technion-IIT, 32000, Haifa, Israel

Alon Hoffman
Department of Chemistry and the Solid State Institute, Technion-IIT, 32000, Haifa, Israel

(Received 14 September 1999; revised manuscript received 31 January 2000)

We propose an approach to modeling the mismatch-induced residual thermal stress in microscopic film/substrate systems using an atomistic simulation. Criteria for choosing model parameters necessary for successful prediction of macroscopic stress-induced phenomena (quantitatively characterized by a reduction in binding energy) are discussed. The model is implemented in a molecular-dynamics simulation of compressive thermal stress at the (100) diamond/substrate interface. The stress-induced binding-energy reduction obtained in the simulation is in good agreement with our model. The effect of sample size and local amorphization on obtained stress values is considered and the maximum on the stress-strain dependence is explained in terms of the ''thermal spike'' behavior. Similarly to results from plasma deposition experiments, the dominant stress-induced defect is found to be the tetrahedrally coordinated amorphous carbon (*ta*-C). At higher film continuities these defects are partially converted into $\langle 100 \rangle$ split interstitials; at lower stresses transformation of a small fraction of *ta*-C into the graphitic sp^2 configuration takes place. The penetration depths and the distribution of the stress-induced defects are determined. The influence of residual stress on diamond thermal conductivity is studied; defects formed due to stress are shown to reduce the thermal conductivity, this effect being partially offset by the counteracting influence of stress on the phonon density of states.

I. INTRODUCTION

The remarkable properties of diamond that include its extreme hardness, high thermal conductivity, transparency, semiconductivity, low coefficient of friction, and chemical inertness make it attractive for a variety of applications.[1] The potential of diamond as an engineering material has considerably increased in the last two decades with the development of advanced chemical vapor deposition (CVD) techniques[2] producing polycrystalline diamond of quality approaching that of the best single crystals.[3] Moreover, CVD makes possible a wide range of products not accessible using bulk diamond.[4–6]

The quality of CVD films is often limited by residual stresses, arising during the growth process. These stresses have been ascribed to the mismatch between the thermal expansion coefficients of diamond and of the underlying substrate (the so-called ''*thermal stress*'')[7,8] and to several factors leading to ''*intrinsic stress*,'' such as the incorporation of nondiamond phases at grain boundaries and the presence of hydrogen and the porosity arising during the growth.[9–11] In films obtained by the CVD technique, thermal stress has been shown to be the main component ($\sim$90%) of the residual stress.[7] A detailed understanding of microscopic processes induced by residual thermal stress, the mechanism for its relaxation, as well as its effect on the structure and properties of diamond, is crucial for predicting reliability and wear resistance of CVD diamond films.

In spite of a large number of experimental analyses of residual stress in CVD diamond films,[7–16] this topic is still not well understood; many questions remain open. For example, not much is known regarding the evolution of defects arising in diamond during the CVD process under conditions of residual stress. Though it is generally known that the application of stress may lead to considerable structural changes in the crystal, such as the formation of defects and other local inhomogeneities,[17] experimental evidence concerning the nature of stress-induced defects in diamond films is still lacking.

The problem of defects arising as a result of stress is closely related to phenomena observed in Raman spectra during the film deposition process. Stress-induced shifts and splittings of the zone-center optical mode of diamond[18] render Raman spectroscopy a technique well suited for the characterization of the developing stresses.[19] Several empirical models relating either shifts[20–23] or splittings[19] to stress values have been derived. However, the behavior of Raman peaks associated with nondiamond phases and defects remains unexplained. In particular, it has been observed that the intensity of the amorphous carbon peak, initially present in the deposited film, first increases and then decreases with the deposition time in correspondence with the evolution of

0163-1829/2000/62(4)/2920(17)/$15.00

film continuity.[7,8,24] This observation, apparently connected to the nature and evolution of defects, has not yet been explained.

The influence of residual stress on thermal conductivity of diamond is of great technological importance. Many applications of CVD diamond are based on its ability to effectively dissipate heat.[3,25] The influence of stress on thermal conductivity can be inferred from the known effect of stress, due both to the change of lattice parameters and as a result of induced defects, on the vibrational spectrum. The relative importance of these two mechanisms can be investigated using the phonon spectrum (PS) method for the calculation of thermal conductivity, discussed in our earlier study,[26] which establishes a direct connection between the phonon spectrum of a dielectric and its thermal properties.

Atomistic simulation in general and molecular dynamics (MD) in particular is a powerful technique for investigating thermal stress with very fine spatial and time resolution, thereby providing information that is difficult or impossible to obtain experimentally. To date, several authors have addressed the behavior of diamond under stress using atomistic simulation techniques. Two studies are of special relevance. Uemura[27,28] studied the behavior of the *bulk* diamond under uniaxial tensile[27] and compressive[28] stress using a modified tight-binding approximation; in particular, the critical strength of perfect diamond was determined. The papers of the group of Pailthorpe and McKenzie[29–37] are more relevant to the present paper. They studied the process of plasma deposition of diamond films using either a modified Stillinger-Weber[29–35] or the Lennard-Jones[36,37] potential, and investigated phenomena that produce compressive stress and allow it to be relieved. In particular, a ''thermal spike,'' defined as a molten zone or simply as the region in which the local structure is significantly distorted,[36] was shown to form following ion bombardment. Above some critical size this spike causes the relaxation of stresses.[30,31,35–37] Another important result is that the compressive stress generated by ion impact induces the formation of tetrahedrally coordinated amorphous carbon (*ta*-C).[30,32,34,38]

The above studies, however, are concerned with the intrinsic component of residual stress prevailing when plasma deposition is used.[30] Recall that when CVD is utilized, thermal stress plays the major role[7] and the aforementioned phenomena, which are likely to result from ion bombardment, may be of little relevance. Here, we present a study based on various experimental results obtained for the CVD diamond films (in particular those of Hoffman and co-workers[7,8,16,24]), thereby placing an emphasis on the thermal component of stress.

We report on MD simulations of diamond deposited on a substrate with a thermal expansion coefficient larger than that of diamond (e.g., silicon), hence producing a compressive mismatch-induced thermal stress. Throughout our paper the Brenner potential[39] is used. The paper is structured as follows: in Sec. II we present the model used for the simulation of thermal stress, film continuity, and experimental conditions. In Sec. III we briefly describe our simulation method and the details of its implementation. In Sec. IV we discuss the reduction of the binding energy due to thermal stress, the effect of sample size, and amorphous inclusions on the value of obtained stresses, the nature, formation mechanism, and the penetration depth of arising defects, and the thermal conductivity of diamond obtained with residual stresses. The conclusions are summarized in Sec. V. The dependence of the mismatch influence on sample size and mismatch factor is analytically derived in Appendix A, and the Rayleigh coefficients for the defects considered here are evaluated in Appendix B.

II. MODELING OF THERMAL STRESS IN A MICROSCOPIC SYSTEM

There are two principal approaches to the MD simulation of stress. In the first (''formalistic'') approach the Hamiltonian of the system is modified with either stress or strain being introduced into the equations of motion.[40–45] In the second group of methods (referred to below as the ''physical'' approach) the particular physical processes that cause the stress are simulated at the atomic level (e.g., the application of an external force[27,28] or the ion bombardment involved in plasma deposition[29–37]). This second way is preferable either when the particular mechanism leading to the appearance of stress is expected to be important, or when the produced stress is inhomogeneous and hence cannot be well modeled by a single general variable. In the case of thermal stress both these factors are relevant.

We describe a model for the ''physical'' simulation of mismatch-induced thermal stress, and discuss important modeling issues related to the small size of the simulation system. Note that this size problem is relevant for all atomistic simulations thereby suggesting that our approach may be applicable to other systems.

Our model also addresses the simulation of the increase of film continuity that is observed during the deposition process. The straightforward approach would be to consider discrete grains with a realistic and continuously increasing size; however, at present such a simulation is impossible for systems with nontrivial potentials,[27] in which sample sizes are restricted to tens of angstroms, whereas the realistic grain size is much larger.[7] To avoid this problem, we propose an alternative method for modeling the increase of film continuity. A qualitative presentation of our model is given below; the corresponding equations are derived in Appendix A.

A. Modeling of stress

The simulated diamond crystal consisted of 512 atoms ($4\times4\times4$ unit cells) interacting via the Brenner potential[39] (see Sec. III for more details). Biaxial thermal substrate stress in the (100) plane was simulated by compressing the two bottom (100) layers (the ''substrate'') by a ''mismatch factor'' f_m in two directions, [010] and [001], coinciding with the x and y axes, respectively (Fig. 1). Accordingly, the mismatch factor

$$f_m \equiv a_s / a_d \tag{2.1}$$

is the ratio of the lattice parameters of substrate (a_s) and diamond (a_d), and the strain tensor in the principal axes is

$$E = \begin{pmatrix} e_x & 0 & 0 \\ 0 & e_y & 0 \\ 0 & 0 & 0 \end{pmatrix}, \tag{2.2}$$

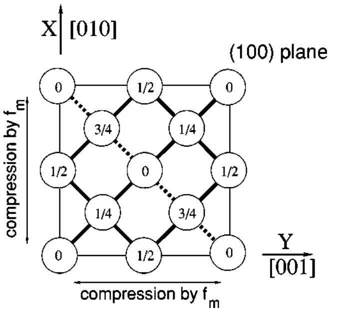

FIG. 1. The (100) diamond surface at which the biaxial compressive stress is applied (unit cell). Numbers indicate the coordinate along the [100] (z) direction in units of the lattice parameter of diamond a_d (positive z direction is into the page). Bonds with atoms of the deepest plane $z=a_d$ (underlying those at $z=0$) are shown by dashed lines.

where $e_x=e_y\equiv -e=f_m-1$.

The substrate atoms were immobilized to prevent expansion by making their masses very large (equal to 10^{11} M_{carbon}). The interactions within the substrate and between the substrate and the diamond film were described by the same Brenner potential[39] used for the bulk diamond (see Sec. III), thus simulating a diamondlike substrate, such as silicon.[9]

The lateral normal stresses (σ_{xx} and σ_{yy}) were calculated by summing forces across an imaginary vertical slice[29] in the yz and xz planes and subtracting the reference values of ideal nonstressed diamond. The reported values of stress are the average of these quantities over the x and y directions.

B. Choice of the mismatch factor: Microscopic correction to macroscopic mismatch factor

At the deposition temperature (T_{dep}=800 °C) it is assumed that there is no mismatch between the diamond film and the substrate ($a_s^{T_{\mathrm{dep}}}=a_d^{T_{\mathrm{dep}}}$).[7] At a lower temperature T, the mismatch factor f_m, which is a result of the difference between linear thermal expansion coefficients of diamond (α_d) and substrate (α_s), can be calculated using the definition of α[46]

$$\left(\alpha_s\equiv\frac{1}{a_s}\frac{da_s}{dT}=\frac{d\ \ln a_s}{dT},\quad \alpha_d\equiv\frac{1}{a_d}\frac{da_d}{dT}=\frac{d\ \ln a_d}{dT}\right)$$

to be

$$f_m(T)\equiv\frac{a_s}{a_d}=\frac{a_s^{T_{\mathrm{dep}}}\exp\left(\int_{T_{\mathrm{dep}}}^{T}\alpha_s dT\right)}{a_d^{T_{\mathrm{dep}}}\exp\left(\int_{T_{\mathrm{dep}}}^{T}\alpha_d dT\right)}$$

$$=\exp\left(\int_{T_{\mathrm{dep}}}^{T}(\alpha_s-\alpha_d)dT\right)\approx 1+\int_{T_{\mathrm{dep}}}^{T}(\alpha_s-\alpha_d)dT. \tag{2.3}$$

The dependence of f_m on T for two substrates, one very similar to diamond (silicon) and another very different (chromium carbide), as calculated with Eq. (2.3), is presented in Fig. 2. This figure shows that even when $\alpha_s-\alpha_d$ is quite large, the mismatch factor is not smaller than 0.99.

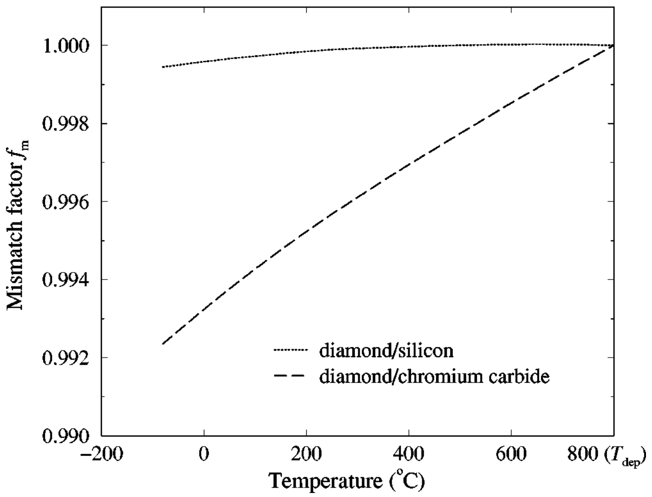

FIG. 2. Mismatch factor f_m as the function of temperature for two substrates calculated by Eq. (2.3). Dependence of diamond and silicon thermal expansion coefficients on temperature, used for the calculation, was taken from Ref. 48; the coefficient of chromium carbide, which is weakly dependent on temperature, was taken equal to 11.7×10^{-6} K^{-1} for the entire temperature range (Ref. 7).

In order to reproduce the influence of mismatch seen in experiments, it would seem appropriate to accept the above value of f_m for our simulations. However, if we quantitatively define the ''influence of mismatch'' either as the average deviation from equilibrium of a bond between the diamond and the nearest substrate atom, $\langle\Delta r\rangle$, or alternatively, as the degree to which the binding energy is reduced due to a mismatch, $\langle\Delta U\rangle$, such a choice of f_m turns out to be incorrect. This is a result of the fact that our simulation system is microscopic in size; contrary to macroscopic systems, where the influence of mismatch is completely determined by the mismatch factor f_m, for microscopic systems it is also dependent on the sample size L.

The general analytical expressions for $\langle\Delta r\rangle=f(L,f_m)$ and $\langle\Delta U\rangle=f(L,f_m)$ are derived in Appendix A with a graphical presentation of these dependencies given in Fig. 3. The behavior of both quantities is highly oscillatory at small L and converges to size independent values as $L\rightarrow\infty$. These large-sample values vary with the mismatch factor in a nonmonotonic manner (see Appendix A); however, in the range of $f_m=0.90-0.99$, this variation is small and corresponds to approximately the same maximal ($\sim 10\%$) weakening of the binding energy for all values of f_m [Fig. 3(b) and Eq. (A36)]. This (10%) is the magnitude of the mismatch influence expected in experiments (at $f_m\approx 0.99$), where the samples are not smaller than hundreds of angstroms (point A in Fig. 3).

However, applying the same ''experimental'' value of mismatch, $f_m=0.99$, to our small sample size, $L\sim 15$ Å, we emerge at the highly oscillatory part of the curves (point B in Fig. 3). At this point the mismatch-induced strain of the bond and the corresponding weakening of the interaction are close to zero—either initially [Fig. 4(a)], or after an easy shift of all atoms, which pushes the nonmatching one out of the sample [Fig. 4(b)]. This cannot happen in large samples, where too many ''internal'' atoms have to be shifted, and the freedom of their movement is too small to enable such ''free surface'' relaxation [Fig. 4(c)].

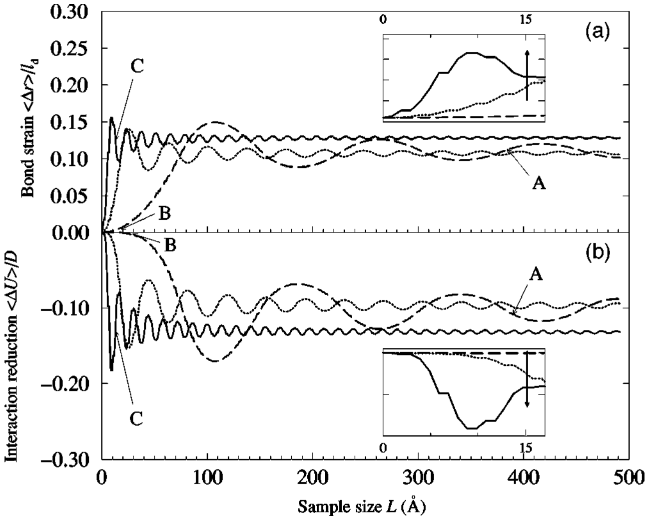

FIG. 3. Dependence of (a) the average bond strain (in units of the diamond bond length, $l_d = 1.54$ Å), calculated using Eq. (A23), and of (b) the reduction of the binding energy per atom (in units of the well depth D), calculated using Eq. (A25), on sample size L, for different values of the mismatch factor: $f_m = 0.90$ (solid line), $f_m = 0.96$ (dotted line), and $f_m = 0.99$ (dashed line). Insets show magnification of the small-sample part of the curves. Arrows on insets indicate the increase of the ''film continuity,'' corresponding to the decrease of the mismatch factor f_m. See Sec. II B for the explanation of the A,B, and C notations.

Consequently, if we would apply the ''experimental'' mismatch factor $f_m \approx 0.99$ to our small sample, we would obtain a mismatch influence much smaller than that obtained in experiment. As shown in Fig. 3, this ''small size effect'' can be compensated by decreasing the mismatch factor with an effect similar to that of increasing the sample size. If, for example, $f_m = 0.90$ is taken, even the small system is located at the saturation limit (point C in Fig. 3) and the interaction is weakened to the same degree ($\sim 10\%$) as in experiment. Thus, in order to obtain the same ''mismatch influence'' as the factor $f_m \approx 0.99$ produces in experiment, in our simulation a smaller mismatch factor such as $f_m \approx 0.90$ is applied.

C. Modeling the increase of film continuity

Scanning election microscopy and micro-Raman studies of the evolution of deposited films have shown[7,8] that the density of diamond particles grows as time advances and reaches a maximum value after 30 min of deposition. A continuous film is obtained after 60 min and, for longer deposition times (120 min), secondary nucleation takes place. This increase of film thickness and continuity leads to the buildup of residual stresses, which has been explained in Ref. 7 as follows. In the case of noncontinuous films, partial stress relaxation is enabled by the relatively large freedom of movement of different parts of the film, presumably the free crystallites surfaces, while in a continuous film the stress cannot relax this way and therefore builds up.

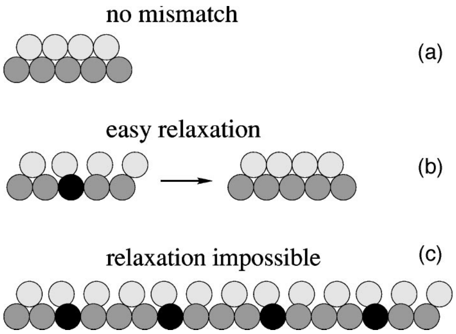

FIG. 4. Scheme of the average bond strain and its relaxation abilities for a small sample (''isolated particle''—a,b) and a large one (''continuous film''—c). Diamond atoms are shown by light gray, substrate atoms in general by dark gray, and substrate atoms with the maximal mismatch are black. For clarity, in this figure the close packing is shown.

As explained above (Sec. II B), this is similar to what happens (Fig. 4) when the $\langle \Delta r \rangle$ and $\langle \Delta U \rangle$ curves achieve the saturation limit, either by increase in the sample size or by decrease of the mismatch factor (insets in Fig. 3). We used the latter method to approximate the effect of increasing film continuity (leading to the buildup of stress) by varying the mismatch factor f_m from 1.0 to 0.9; the latter value is expected to give results, qualitatively similar to those of a macroscopic, continuous film with the maximal thermal stress. Although this approach appears artificial (it is based on the *mathematical* equivalence between the impact of decreasing mismatch factor and increasing sample size), using the more realistic approach of varying sample size is nonpractical due to the large increase in demands on computational resources.

D. Modeling the experimental set up (temperature regime and initial amorphization)

In order to mimic the experimental conditions of diamond CVD, our ''computer experiment,'' unless stated otherwise, included three stages:

1. ''Deposition''

At this first stage the diamond/substrate system was equilibrated for 2.5 ps at the deposition temperature (a typical value[7–9,47] of $T_{\mathrm{dep}} = 800\,^\circ\mathrm{C}$ was used). Some *initial* ''local'' amorphization of diamond near the diamond/substrate interface, caused by thermal fluctuations and facilitated by the attachment of the diamond to a rigidly fixed substrate resulting in the ''growth strain,''[11] was already present in our sample before any mismatch was introduced. This reproduces experimental CVD conditions, where such nondiamond phases were detected immediately after the deposition, in the ''as-grown'' film.[7,19]

2. ''Cooling'' and equilibration

The system was then ''cooled'' to room temperature (25 °C) at which the experimental measurements are made. At this stage the whole lattice was compressed in accordance with the thermal expansion coefficient of diamond[48] (cooling from 800 to 25 °C results in the change of the lattice parameter from 3.576 to 3.567 Å). The substrate part was additionally compressed by the mismatch factor f_m, thus simulating the difference in thermal expansion coefficients of diamond and substrate. An appropriate choice of f_m is discussed above (Secs. II B and II C). The cooled system was then equilibrated during 2.5 ps.

3. Data collection

During this stage various properties of the equilibrated system (phonon spectrum, radial distribution function, thermal conductivity, etc.) were ''measured'' during 5 ps (this time has been shown to be appropriate for obtaining the phonon spectra with sufficient resolution[26]).

III. SIMULATION METHOD

The evolution of the diamond/substrate system was simulated using the MD technique efficiently implemented on a parallel high-performance computer as described in Ref. 49. We used 16 processors of an SP2 for 20 h for each run, making some 25 runs in the course of the project. The equations of motion were integrated for 10 ps by the ''leap-frog'' algorithm[50,51] with an integration time step of $\Delta t=5\times10^{-5}$ ps.

The simulated system consisted of 512 carbon atoms ($4\times4\times4$ unit cells, 16 monoatomic layers in each of [100], [010] and [001] directions) with minimum-image periodic boundary conditions.[50,51] The periodic boundary conditions allow us to overcome the effect of surface on the calculated properties.[50] They do not increase the size of the system to make it ''macroscopic'' since the periodicity suppresses any density waves with a wavelength greater than the simulation box.[50] The fact that an atom relaxing via a ''free surface'' [Fig. 4(a)] enters through the opposite face of the simulation box does not influence relaxation; the simulation system remains ''small,'' and the above model holds. Similarly, the ''grain size'' in the calculation of the thermal conductivity (see Sec. IV E) should be considered to be equal to the length of the simulation cell.

Interatomic interactions were described by the potential of Brenner,[39] which is believed to accurately model diamond and various carbon forms intermediate between diamond and graphite, as well as defects with various types of hybridization; this is important for the study of stress, which produces a variety of defects. The details of our implementation of this potential are given in Ref. 26.

The required temperature regime (see Sec. II D) was maintained by the periodic rescaling of all atomic velocities followed by equilibration of the system[50] (the reasons for such a choice of temperature maintenance method are explained in Ref. 52).

IV. RESULTS AND DISCUSSION

A. Reduction of binding energy as a result of thermal stress

As defined above, the influence of thermal stress can be quantitatively characterized by the reduction of binding energy caused by stress-induced mismatch. This quantity, measured immediately after the mismatch was introduced (''as-grown'' film) and again after the relaxation, is plotted in Fig. 5.

Initially (circles in Fig. 5), the reduction of the binding energy is rather large and reaches approximately 0.6 eV/atom for the largest considered mismatch, $f_m=0.90$. This reduction is due both to mismatch and to a small number of defects, present already after the deposition stage.

When the sample is allowed to relax (triangles in Fig. 5), the accounted reduction of the binding energy becomes smaller since the system has time to adjust itself to the optimal structure. The agreement of these simulation values of the binding energy reduction with those predicted by our theoretical model [crosses; calculated using Eq. (A25)] is very good considering the roughness of the model and the fact that the modeled values were averaged over the sample thickness under the assumption that the mismatch influence distributes uniformly over the entire sample, while in reality this is not so (see Sec. IV D). For high mismatches ($f_m<0.94$) the reduction of binding energy is due not only to the mismatch itself, but also to the stress-induced formation of defects (Sec. IV C) not taken into account in the model but accounted by the simulation; hence a larger and a more monotonous reduction of energy in the simulation compared to that given by the model.

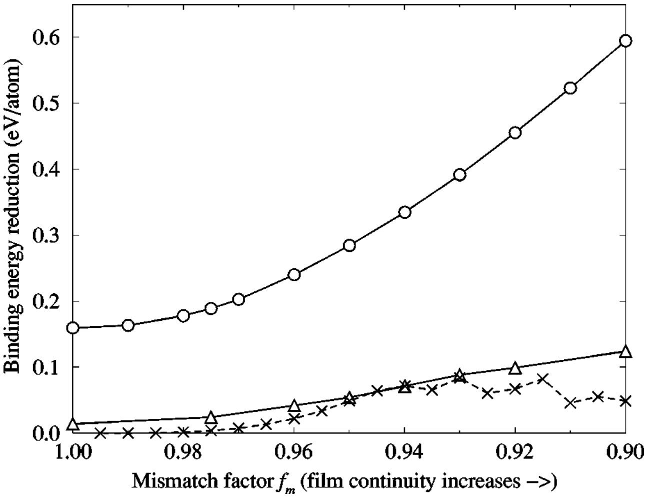

FIG. 5. Reduction of the binding energy due to mismatch: immediately after the deposition stage, ''as-grown'' film (circles), and after the relaxation (triangles). Model values (calculated using Eq. (A25) and divided by 8 to consider that the mismatch located in 2 layers acts over 16 and not 2 layers, as was assumed in the model) are also shown for comparison (crosses).

B. Effect of sample size and local amorphization on obtained stresses

To single out the ''pure'' dependence of measured stress on the value of substrate strain, we considered the samples subjected *only* to a mismatch (without preliminary deposition stage heating resulting in initial amorphization). The initial substrate layer stress in these samples is presented in Fig. 6 (solid line). As expected, the mismatch-induced thermal stress is compressive. The slope of a linear fit to the curve allows us to evaluate the biaxial Young modulus:[7,19,53]

$$\frac{E}{1-\nu}=\sigma/e\approx469\ \text{GPa}, \tag{4.1}$$

where E is the Young modulus and ν is the Poisson ratio. This result is almost three times smaller than the value from the literature [1345 GPa (Refs. 7 and 19)], corresponding to $E=1050$ GPa (Ref. 54) and $\nu=0.219$. This discrepancy is most probably the result of the decrease in the influence of mismatch in the case of small samples, discussed in Sec. II B. The literature value of the elastic modulus, suitable for

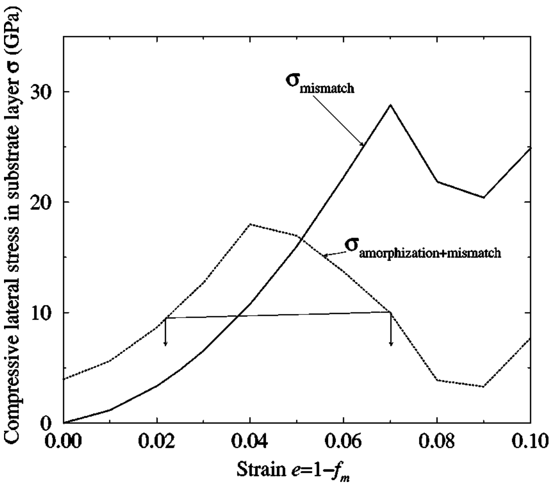

FIG. 6. Initial lateral stress σ in the substrate layer as a result of the strain e for an ideal crystal (solid line) and for defect-containing samples obtained by the simulated CVD (dotted line); the thin line with arrows indicates the stress below which the graphitic sp^2 defects can be formed.

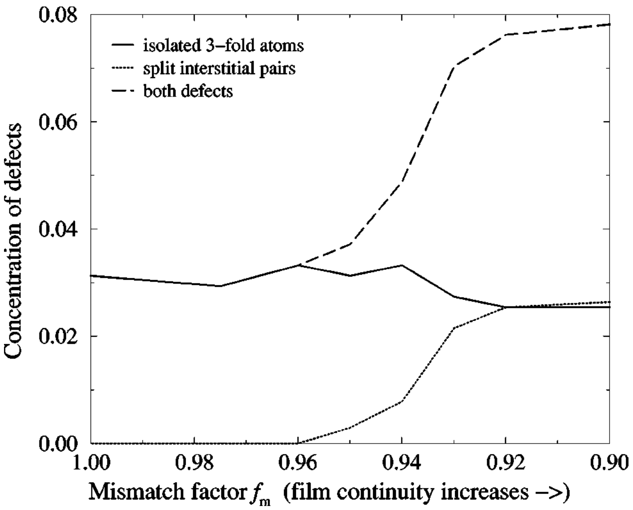

FIG. 7. Evolution of defects concentration with the increase of mismatch (corresponding to the increase of the film continuity) calculated based on coordination numbers. This figure does not reflect the difference between the ''intermediate tetrahedrally coordinated amorphous carbons,'' *ta*-C, and the sp^2 atoms in graphitic configuration (see the text); both these defects are classified as ''isolated three-fold atoms.''

the *bulk*, was determined experimentally for large samples located in the ''saturation'' region (point *A* in Fig. 3), while the stress-strain relationship in a *thin* film (or a *monoatomic* substrate layer for which our estimations were made) is not as straightforward,[11,55] and the influence of mismatch produced by the same strain is expected to be much smaller (point *B* in Fig. 3). This phenomenon is similar to an experimentally known fact that smaller diamonds (in which the ability to relax is higher) exhibit greater strength than larger ones[56] and yield when larger samples would have cracked.[57,58] Additional confirmation is given by the results of other simulations of diamond, e.g., those of Uemura[28] who obtained elastic constants underestimated by a factor of 1.34 even for a relatively large sample (4000 atoms).

The maximum in the stress-strain dependence can be explained in terms of a ''thermal spike'' behavior, observed in ion bombardment (plasma deposition) experiments[30] and substantiated theoretically.[31,35–37,59] The thermal spike is defined as a zone in which a *local* melting followed by rapid chilling had occurred due to a highly energetical ion impact;[30,36] roughly speaking, it is the region in which local structure is significantly distorted.[36] With increasing impact energy the thermal spike region grows; starting from some critical value of energy, it becomes large enough to allow the relief of stresses, thus giving rise to a maximum in the dependence of stress on impact energy.[29,30] A similar phenomenon can be expected also for thermal stress resulting from the mismatch. The larger the mismatch, the more defects are formed (see Sec. IV C); when some critical concentration of defects is achieved, a partial relaxation of stress on these defects becomes possible. According to Fig. 6, this happens when the strain e achieves a value of 0.07 $(f_m=0.93)$.

In a realistic system produced by the deposition at 800 °C and then cooled (dotted line in Fig. 6), some initial amorphization is present in addition to mismatch (see Sec. II D). Such nondiamond inclusions are known to cause an intrinsic stress[9,11,30] which can be either compressive[30] or tensile.[9] At small strains (before the critical concentration of defects is obtained) the difference between the stress value with and without this amorphization is positive; hence in our case the intrinsic stress is compressive. However, due to the presence of some defects already at zero mismatch, the apparent critical concentration of defects necessary for a stress to relax is achieved much earlier (at $e=0.04$, $f_m=0.96$) than in the perfect crystal, and the reduction of stress is considerably larger due to its more efficient relaxation. As seen in Fig. 7, the apparent critical concentration of defects is equal to ~3.3 at. % (the value corresponding to $f_m=0.96$). The distorted crystal with $f_m=0.96$ is visualized in Fig. 8 which shows that, in addition to the near-substrate layers, a significant internal region is distorted.

After passing the maximum, at $f_m\approx0.92$ $(e\approx0.08)$, the concentration of defects reaches saturation and stops growing with mismatch (Fig. 7). For a further increase of mis-

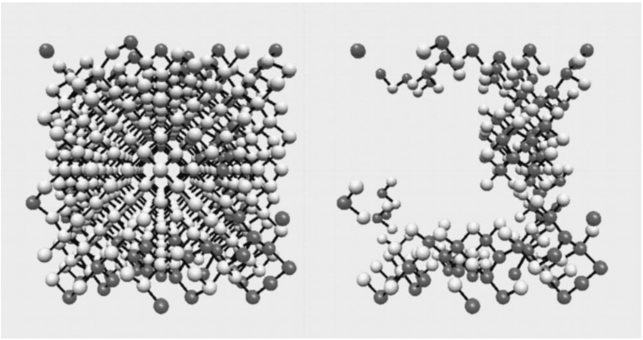

FIG. 8. Distortion of the diamond crystal obtained at 800 °C (resulting in initial amorphization) with mismatch $f_m=0.96$ (strain $e=0.04$): the whole crystal (left) and the distorted region (right). Nondistorted four-fold diamond atoms are shown by white, while all atoms with coordination different from four, as well as the compressed substrate atoms, are shown by black. The distortion appears not only in the lower, but also in the upper layer of the sample, due to the use of periodic boundary conditions.

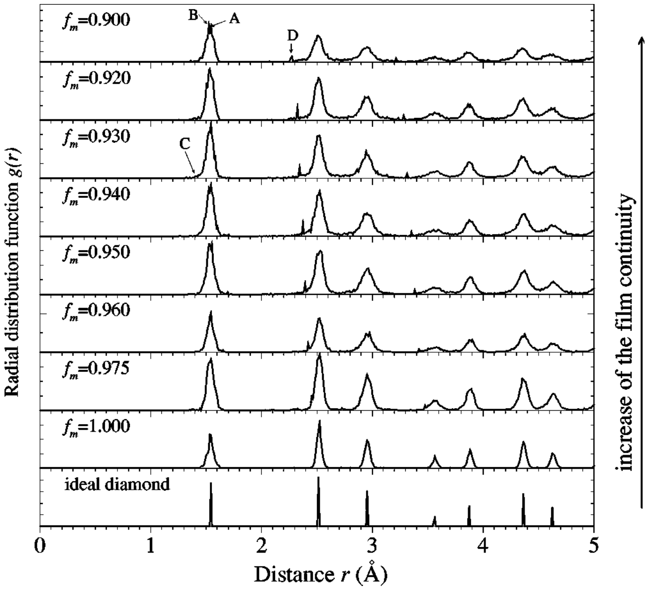

FIG. 9. Evolution of radial distribution function with the increase of mismatch (corresponding to the increase of the film continuity). Notation of peaks: A—ideal diamond, B—tetrahedral amorphous carbon, *ta*-C, C—three-fold graphitic sp^2 atoms, and D—split interstitials.

match, the relief of stress due to this concentration of defects becomes insufficient to overcome the buildup of stress due to a larger strain; hence, in this case, stress again increases with increasing strain (Fig. 6).

C. Formation of defects as a result of thermal stress

Three types of defects were found to form as a result of the thermal stress: (1) isolated atoms with approximately three-fold coordination, intermediate between the diamond sp^3 and the graphite sp^2 configurations (referred to as ''tetrahedrally coordinated amorphous carbons,'' *ta*-C,[30] or as ''intermediate carbons''[60]), (2) isolated three-fold atoms possessing the graphitic sp^2 configuration, and (3) split interstitials, which can be defined as dumbbell pairs of three-fold atoms.[61]

The formation and the evolution of these defects with increase in mismatch (corresponding to the buildup of stress and to increase in film continuity) were followed using several quantities: the concentration of each type of defect (Fig. 7), the radial distribution functions (RDF) (Fig. 9), and the phonon spectra (density-of-states) calculated by Fourier transformation of the velocity-velocity autocorrelation functions[62] (Fig. 10). The concentration curves were calculated based on atomic coordination numbers; these numbers are integer[63] and hence do not allow us to exactly distinguish the tetrahedral amorphous carbon [whose coordination number is 3.7 (Refs. 30 and 38)] from the perfect four-fold diamond, on one hand, and from the three-fold atoms in the sp^2 configuration on the other hand. For the following, we will refer all atoms having less than four neighbors inside the cutoff radius [$r_c = 2$ Å (Ref. 39)] and hence considered ''three-fold'' to the class of intermediate carbons. However, we will bear in mind that their coordination is not *exactly* equal to 3 and their configuration is not *necessarily* sp^2; in order to decide whether this is the case or not, additional evidence will be used. The radial distribution function was used to extract information both on the bond length (given by the nearest-neighbor distance r_1) and on the bond angle θ obtained from the ratio of the first- and second-neighbor distances:[30] $\theta = 2\arcsin(r_2/2r_1)$. In summary, the results presented in Figs. 7–10 allow us to suggest the following mechanism of defect evolution.

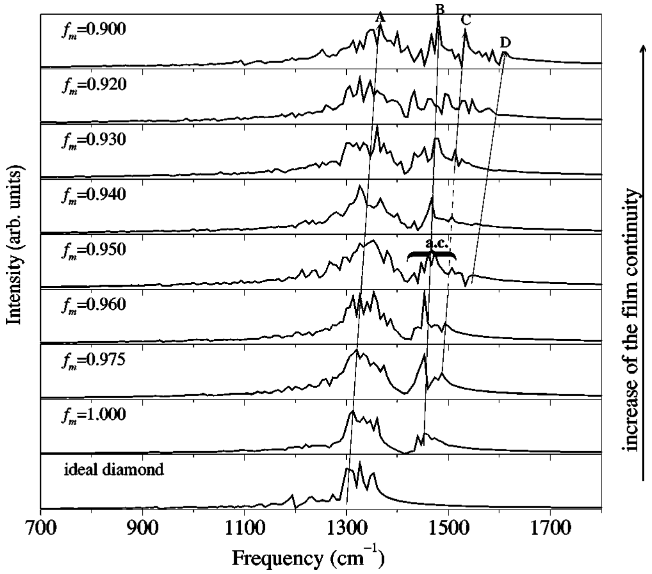

FIG. 10. Evolution of phonon spectrum with the increase of mismatch (corresponding to the increase of the film continuity). Notation of peaks: A—ideal diamond, B—tetrahedral amorphous carbon, *ta*-C, C—three-fold graphitic sp^2 atoms, and D—split interstitials; a broad feature attributed to both kinds of isolated three-fold defects, *B* and *C*, and referred to as an ''amorphous carbon peak'' is marked by ''a.c.''

1. Breaking of diamond bonds—formation of ''intermediate tetrahedral amorphous carbons,'' ta-C

First, when the mismatch is small (loosely corresponding to a low film continuity), the dominant defects are atoms with an approximately three-fold coordination (Fig. 7), resulting from the breaking of one of the diamond bonds. For these defects the formation energy is relatively low: according to Ref. 17, the energy of a single C-C bond (to be broken) is equal to 3.6 eV.

As noted above, in order to decide whether this defect is the tetrahedral amorphous carbon (*ta*-C) whose coordination number is 3.7 (Refs. 30 and 38) or the ''true'' three-fold atom with the graphitic sp^2 configuration, additional evidence is obtained from the radial distribution functions and phonon spectra. Based on the RDF (peak *B* in Fig. 9) analysis, the defect in question corresponds to the bond length $r_1 = 1.525$ Å and the bond angle $\theta = 111°$; these values are almost identical to those reported for the tetrahedral amorphous carbon, $r_1 = 1.53$ Å and $\theta = 110°$.[30] In the phonon spectrum, this defect gives rise to the local mode vibration ~ 1450 cm^{-1} (peak *B* in Fig. 10); similar peaks in the 1400–1500 cm^{-1} region were observed and attributed to various C-C vibrations in amorphous diamond,[64] in particular, to the stretching vibrations between the four-fold and three-fold atoms[62] accounted, e.g., in case of a vacancy.[65,66]

The formation of *ta*-C defect as a result of compressive stress was experimentally and theoretically proven for plasma deposition experiments[30,38] in which the dominating component of stress is intrinsic.[30] The above data, obtained from our simulation, serve as an unequivocal evidence of the compressive-stress-induced formation of this defect also under CVD conditions promoting the development of thermal rather than intrinsic stress.[7]

The presence of a small concentration of this defect even in samples with no mismatch ($f_m = 1.0$) is accounted for by an initial ''local amorphization'' resulting from the deposition at high temperature.

2. Conversion of a part of the sp^3 ta-C to the graphitic sp^2 configuration

Stabilization of the diamondlike *ta*-C defect compared to the sp^2 graphitic defect under the conditions of compressive stress is consistent with the phase diagram of carbon,[67] showing that at higher pressures the diamond state is favorable. However, when the stress is not too large, the conversion of some sp^3 *ta*-C defects to the graphitic sp^2 configuration becomes possible.[68] The presence of the small 1.41 Å peak and of the bond angle $\theta = 126°$ in the radial distribution function, as well as of the 1533 cm^{-1} feature in the phonon spectra (peaks *C* in Figs. 9 and 10) indicate that the graphitic sp^2 configuration exists approximately for $f_m \geqslant 0.975$ and for $f_m \leqslant 0.930$ (compare to the corresponding values 1.45 Å, 120° (Ref. 69) and 1582 cm^{-1} (Ref. 62) for graphite). This can be explained based on the nonmonotonic stress-strain relationship, discussed in Sec. IV B. When the strain is small ($f_m \geqslant 0.975$, $e \leqslant 0.025$) the stress is rather low, and the sp^2 configuration can form. When the strain is large enough, the concentration of defects approaches the critical value enabling a partial relaxation of stress, and at $f_m \leqslant 0.930$ ($e \geqslant 0.070$) the stress again becomes low enough to make the existence of the sp^2 configuration possible (see Fig. 6 where the stress below which the graphitic defect exists is shown).

3. Additional stabilization of above configurations at higher stresses—formation of split interstitials

The predominant *ta*-C defect is stable enough[38] and present up to the highest considered mismatches. However, this defect, being intermediate between the diamond and the (less dense) graphite configuration, requires more volume than the perfect diamond atom would require; indeed, its fractional volume difference relative to diamond is positive, $p_{ta\text{-C}} \approx 0.166$ (see Appendix B). Yet more considerable is this volume difference for the second defect, the sp^2 graphitic carbon ($p_{sp^2} \approx 0.552$). Therefore, accumulation of both *ta*-C and sp^2 graphitic carbon defects (which can be commonly referred to as *isolated* three-fold atoms) with the increase of mismatch requires a volume expansion of the crystal, experimentally known as ''swelling.''[70–72]

As the continuity of the film increases, it becomes more difficult to gain the required additional volume. This causes combining of some of the isolated three-fold atoms into pairs with a stabilization corresponding to the formation of split interstitial defects (Fig. 7). These are presumably $\langle 100 \rangle$ split interstitials, known to be the most stable point defects in diamond.[73,74] As shown in Appendix B, this new defect is more compact than both types of isolated three-fold coordinated defects ($p_{\mathrm{si}} \approx 0.157 < p_{ta\text{-C}} \leqslant p_{sp^2}$) and is hence consistent with the more continuous system with less degrees of freedom.

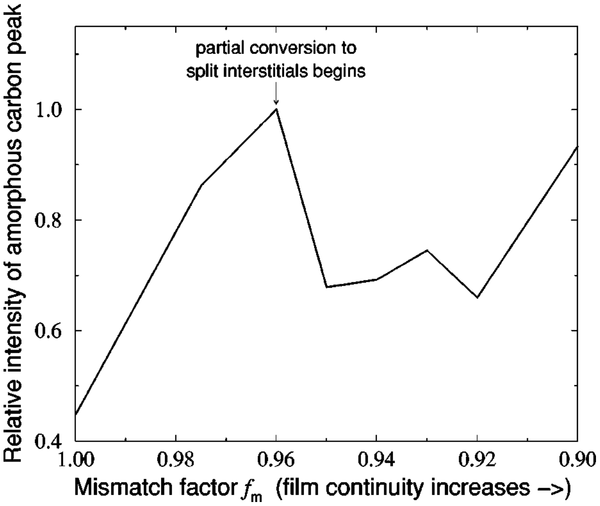

FIG. 11. Intensity of the ''amorphous carbon'' peak with respect to the main diamond peak (*A* in Fig. 10), calculated based on Fig. 10.

The formation energy of $\langle 100 \rangle$ split interstitial, 16.5–16.6 eV,[73,75] is higher than that of the isolated three-fold atom, explaining the absence of these defects at low stresses, i.e., at small mismatches ($f_m > 0.960$) (Fig. 7). When the split interstitial defect is formed, the radial distribution function starts to exhibit new, nondiamond, peaks, such as that located at about 2.425 Å (peak *C* in Fig. 9). As the compressive stress builds up, the defect stabilizes, and this peak evolves towards smaller distances; its value 2.268 Å at $f_m = 0.90$ is close to the distance 2.129 Å between one of the central atoms of the $\langle 100 \rangle$ split interstitial and the terminating dumbbell atom farthest from it for the split interstitial configuration predicted in Ref. 26.

Conversion of a part of the isolated three-fold atoms into split interstitials becomes apparent also when looking at the phonon spectra (Fig. 10): as the film continuity increases, a new local peak (D), evolving towards 1607 cm^{-1} and most likely attributed to the $\langle 100 \rangle$ split interstitial,[65] appears.

The proposed mechanism of defect evolution provides an explanation for the experimental behavior of the amorphous carbon peak in Raman spectra.[7,8] In our case, as the film continuity increases, the intensity of the broad ''amorphous carbon'' feature, located at $\sim$1420–1560 cm^{-1} and attributed to two kinds of isolated three-fold defects (Fig. 11), first increases with the growth of the total concentration of these defects ($f_m \geqslant 0.960$, Fig. 7), and then decreases, when some of these defects convert to split interstitials and their concentration reduces ($f_m < 0.960$, Fig. 7);[76] a similar behavior was observed in experimental Raman spectra.[7,8]

Finally, two additional features of the evolution of the RDF and phonon spectrum with the increase of mismatch should be mentioned. First, the higher the compressive stress, the smaller the stable lengths of all bonds [note, for example, the downward shifting of the aforementioned split interstitial line, initially located at 2.425 Å (Fig. 9)]. Increase

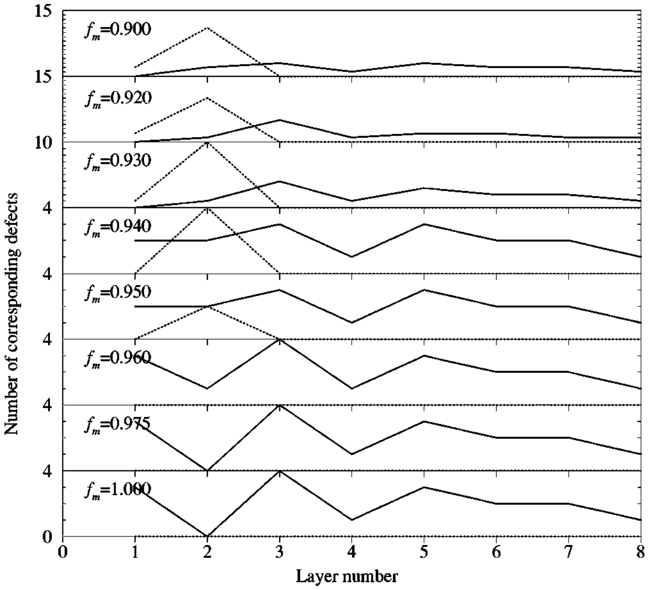

FIG. 12. Penetration depth of stress-induced defects: number of isolated three-fold atoms—''intermediate carbons'' (solid line) and split interstitials (dotted line)—as a function of the layer number. The numbering of layers starts from substrate.

of the compressive stress also causes the upward shift and splitting of the diamond (''*A*'') peak in phonon spectrum (Fig. 10). Second, as the stress builds up, stress-induced defects develop, and the order of the structure decreases (it becomes more amorphous); as a result, the RDF peaks become broader and more ''grassy'' (Fig. 9).

D. Depth of the defects penetration

The penetration depth of various defects can be obtained by mapping their concentrations along the direction normal to the diamond/substrate interface (Fig. 12). This figure demonstrates that the effect of substrate stress on the crystal structure is very deep: when allowed to relax, the defects, initially located near the substrate/diamond interface, expand over the whole crystal, though their distribution remains nonuniform. At small mismatches the defects are the ''intermediate carbons'' (isolated three-fold carbon atoms); the further from substrate, the smaller is their concentration. At larger mismatches, a considerable proportion of these defects turn into split interstitials (see Sec. IV C). In this case, the split interstitials form predominantly near the substrate/diamond interface where the stress is maximal, while the remaining ''intermediate carbons'' (requiring more volume) concentrate in deeper, less compressed, layers.

In experiment the presence of defects can be analyzed using the full width at half maximum (FWHM) of the band-center phonon peak in Raman spectra: a decrease in the degree of crystallinity (increasing defects or amorphicity) is known to increase the value of FWHM.[13] Unfortunately, the penetration depths deduced experimentally based on FWHM cannot be quantitatively compared to our results, since the former are extremely sensitive to the deposition conditions and to the film thickness and orientation. However, the measurements of Sails *et al.* for the $\langle 100\rangle$ oriented film[13] qualitatively confirm our conclusion about the defects propagating deep enough and affecting the whole film.

E. Thermal conductivity of diamond with residual stresses

As demonstrated in Ref. 26, the direct MD calculation of thermal conductivity is considerably affected by the size of the simulation system and by the method of temperature maintenance. Contrary to this, the PS method developed in Ref. 26 is practically insensitive to these factors and gives the correct values of thermal conductivity in the whole temperature range for which experimental data are available. This method is based on the following expression for the thermal conductivity of dielectrics:[17,77]

$$\kappa=\frac{\hbar^2 v^2}{3kT^2 V_{\mathrm{mol}}}\int_0^{\omega_R}\tau(\omega)D(\omega)\frac{\omega^2 e^{\hbar\omega/kT}}{(e^{\hbar\omega/kT}-1)^2}d\omega, \quad (4.2)$$

where T is the temperature, v is the average velocity of sound in the crystal, V_{mol} is the molar volume, ω_R is the maximal frequency up to which the integration is accomplished (it corresponds to the wave vector $\mathbf{k}=0$), $D(\omega)$ is the normalized mode density at frequency ω, and $\tau(\omega)$ is the relaxation time comprising all mechanisms participating in the phonon scattering.[77,78] Under the assumption that the scattering mechanisms are independent one from another, the scattering rates of individual mechanisms are additive,[3] and include (in our case) relaxation due to Umklapp processes (τ_U^{-1}), grain boundaries (τ_{gb}^{-1}), and point defects, earlier shown to include the tetrahedrally coordinated amorphous carbon atoms, *ta*-C ($\tau_{ta\text{-C}}^{-1}$), the split interstitials (τ_{si}^{-1}), and the isolated sp^2 graphitic carbons ($\tau_{sp^2}^{-1}$):

$$\tau^{-1}(\omega)=\tau_U^{-1}(\omega)+\tau_{gb}^{-1}(\omega)+\tau_{ta\text{-C}}^{-1}(\omega)+\tau_{\mathrm{si}}^{-1}(\omega)+\tau_{sp^2}^{-1}(\omega). \quad (4.3)$$

Based on the intensity of those RDF and PS peaks, which correspond to the latter defect (Figs. 9 and 10), its concentration is rather low, and the concentration of the ''isolated three-fold'' atoms can be attributed to the *ta*-C defect alone; hence

$$\tau^{-1}(\omega)\approx\tau_U^{-1}(\omega)+\tau_{gb}^{-1}(\omega)+\tau_{ta\text{-C}}^{-1}(\omega)+\tau_{\mathrm{si}}^{-1}(\omega). \quad (4.4)$$

The phonon density $D(\omega)$ was extracted from the phonon spectra (Fig. 10). The expressions for each of the relaxation mechanisms present in Eq. (4.4), as well as the parameters necessary for Eqs. (4.2)–(4.4), were taken from Ref. 26. The Rayleigh coefficients I for the three types of defects not considered in Ref. 26 are evaluated in Appendix B.

The above expressions show that, in principle, the influence of residual stress on thermal conductivity can be inferred in three possible mechanisms: (1) effect of stress on the phonon density-of-states, $D(\omega)$, due to the change of the lattice parameters, (2) appearance of the stress-induced defects serving as an additional mechanism of phonon scattering [appearance or increase of the point defects terms $\tau_{ta\text{-C}}$ and τ_{si} in Eq. (4.4)] and (3) modification of the density-of-states $D(\omega)$ by defects.

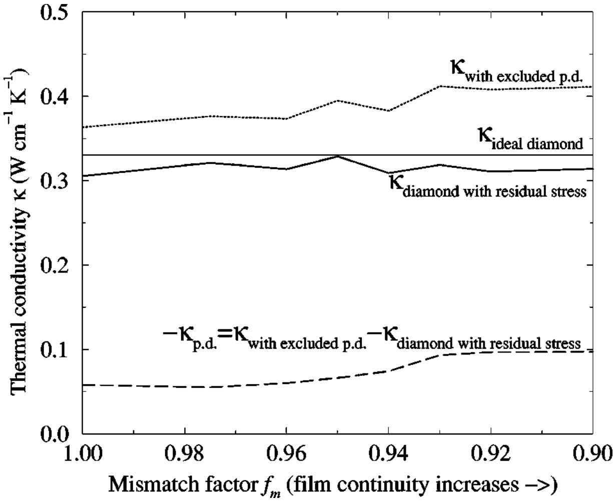

FIG. 13. Thermal conductivity of diamond with residual stress at room temperature (solid line), and its components resulting from point defects (''p.d.'') (dashed line) and from the rest scattering mechanisms (dotted line). Thermal conductivity of ideal diamond is shown for comparison (thin-solid line).

Of these mechanisms, the third does not occur: as shown in Fig. 10, the defects in question do not noticeably affect the spectrum in the quasilocal frequency region ($\omega < \omega_R$), while the local vibrations with frequencies lying above the maximum possible frequency of pure diamond are unable to propagate through the crystal[79] and hence have no effect on its thermal properties. The influence of two other mechanisms is analyzed in Fig. 13.

Change of the thermal conductivity due to the ''pure'' first mechanism [effect of stress on $D(\omega)$] can be isolated by omitting the terms resulting from the relaxation on point defects, i.e., accepting $\tau^{-1} = \tau_U^{-1} + \tau_{gb}^{-1}$ (dotted line termed $\kappa_{\text{with excluded p.d.}}$ in Fig. 13). The figure demonstrates that in this case (if there were no scattering on point defects), the thermal conductivity of diamond under residual stress would be higher than that of ideal diamond, $\kappa_{\text{ideal diamond}}$ (thin-solid line). This would-be increase is accounted for by the fact that compressive stress shifts the maximum frequency upwards, thus enhancing the frequency region in which the phonons can propagate.

However, the true thermal conductivity of diamond with residual stress, $\kappa_{\text{diamond with residual stress}}$ (thick-solid line) is lower that that of ideal diamond. This reduction is due to the second route of the stress influence, namely, to the appearance of defects serving as an additional mechanism of the phonon scattering. The extent to which these defects reduce the thermal conductivity results from the interplay of two factors: the type of prevailing defects and their concentration. On one hand, as the mismatch increases and the stress builds up, the concentration of defects grows (Fig. 7), and the defect-induced reduction of thermal conductivity must become stronger. On the other hand, the buildup of stress was shown to cause the conversion of some of the ''intermediate carbon'' defects to more compact split interstitials, possessing the lower Rayleigh coefficient per single defect (9.31 instead of 9.84, see Appendix B), and hence scattering the phonons less intensively. However, the difference in Rayleigh parameters is rather small, and the latter effect is negligible, so that the resulting degree of the thermal conductivity reduction by point defects, $-\kappa_{\text{p.d.}}$, grows with their concentration, i.e., with the increase of mismatch (dashed line in Fig. 13).

The obtained numerical values of thermal conductivity cannot be directly compared to experiment since, to the best of our knowledge, conductivity of such small samples ($\sim$14 Å), as well as that measured under stress, was never reported in the experimental literature. However, the good agreement exhibited when the applied method was tested on large ideal samples,[26] suggests that the results presented here are also correct.

V. CONCLUSIONS

(1) A model for the atomistic simulation of macroscopic thermal residual stress in microscopic film/substrate systems was presented. In this model the mismatch between the film and underlying substrate, resulting from the difference in their thermal expansion coefficients, was simulated using substrate compression by a factor f_m. The dependence of the mismatch influence (quantitatively defined as the binding energy reduction due to mismatch) on the mismatch factor f_m and sample size L was derived analytically.

Using the dependence of the mismatch influence on L, it was demonstrated that in small (simulated) systems the influence of a given level of mismatch is considerably less than that produced in large (experimental) samples by the same value of mismatch. The reason for this lies in a larger freedom of movement in the small sample, which enables free-surface relaxation of stress. This freedom can be reduced either by increasing the sample size (this happens, e.g., when the film continuity grows with the deposition time) or by introducing a decrease in the mismatch factor thereby producing effects similar to those obtained when increasing the sample size.

Two conclusions can be drawn from the similar effect of increasing the sample size and that of decreasing the mismatch factor. First, in order to produce the same influence of mismatch as is obtained in a macroscopic experiment, in a microscopic system one should use mismatch factors considerably smaller than the realistic ones. Second, the increase of the film continuity, corresponding to reduction in free-surface relaxation and increase in compressive stress, can be semiquantitatively modeled using the continuous decrease of the mismatch factor. This approach is favorable compared to the direct increase in size of a simulated system; such an increase is limited by computer resources that currently render realistic sample sizes unachievable.

(2) The model was applied in the simulation of compressive thermal stress at a (100) diamond surface using the molecular-dynamics technique; the resultant binding-energy reduction was calculated. Initially, when mismatch was introduced, the energy reduction amounted to 0.6 eV/atom for the largest mismatch studied, and became almost five times smaller when the system was allowed to relax. The value of the binding-energy reduction in the relaxed system agrees well with that predicted by our theoretical model except when applying large mismatches that lead to the formation of mismatch-induced defects, not accounted for in the model; these noticeably contribute to the binding-energy reduction.

(3) The biaxial Young modulus, determined from the obtained stress dependence on strain, was found to be smaller than the corresponding literature value. This was explained in terms of the smaller size of the simulation system, which causes a reduction in the mismatch influence thereby favoring stress relaxation and making the macroscopic literature value inappropriate for microscopic simulation. This conclusion is consistent both with our theoretical model and with the results of other simulations.[28] Though, to the best of our knowledge, experimental values of elastic moduli for such small samples are unavailable, the existing experimental data (e.g., a lower strength of large diamonds compared to the smaller ones in which the ability to relax is higher) indirectly confirm this result.[56–58] An underestimation of elastic moduli should be taken into account in all small-system size simulations.

A maximum was observed in the stress-strain relationship. This phenomenon was explained by the fact that for large mismatches the concentration of defects achieves some critical value allowing a partial relaxation of stresses, similarly to the ‘‘thermal spike’’ behavior observed in ion bombardment experiments in which a maximum of the stress-impact energy dependence was obtained.[30,31,35–37] This suggests that, although the origin of stress is different in two cases (the mismatch-induced thermal stress in our ‘‘CVD experiments’’ and the impact-induced intrinsic stress in plasma deposition[30]), the mechanism of stress relaxation is the same. Amorphous inclusions and internal defects, arising as a result of thermal stress, were shown to cause a compressive intrinsic stress.

(4) The evolution of crystal structure with increasing film continuity was investigated. Three types of defects were found to form as a result of stress.

At low film continuities the prevailing defect was shown to be an isolated atom with an approximately three-fold coordination. In agreement with plasma deposition experiments[30,38] in which defects originated from an *intrinsic* compressive stress, in our simulated CVD experiment, resulting mainly in *thermal* stress, this defect was shown to be the tetrahedrally coordinated amorphous carbon *ta*-C whose configuration is intermediate between diamond and graphite, rather than the graphitelike sp^2 carbon. Interestingly, for low enough stresses, an insignificant concentration of the graphitelike sp^2 carbon defects was also found. For large film continuity values, both of these defects were shown to be partially converted into $\langle 100\rangle$ split interstitials.

These transformations were interpreted in terms of phase diagrams and relative volumes and were found to be consistent with experiment. In particular, the proposed mechanism explains the time evolution of the ‘‘amorphous carbon’’ peak in Raman spectra, observed during the CVD of diamond.[7]

(5) The penetration depth of the stress-induced defects was studied. It was demonstrated that the effect of stress on the crystal structure is long ranged: when allowed to relax, the stress-induced defects, initially located near the substrate/diamond interface, propagate over the whole crystal. When both split interstitials and ‘‘intermediate carbons’’ are present, the former concentrate near the substrate/diamond interface where the stress is maximal, and the latter remain predominantly in deeper layers.

(6) The influence of residual stress on thermal conductivity was studied by the PS method.[26] The residual thermal stress was shown to reduce the diamond thermal conductivity, this reduction being due to the formation of stress-induced defects, leading to additional phonon scattering. This effect, growing with the concentration of defects, counteracts the effect of stress on the phonon density-of-states, namely, the enhancement of the region of phonon propagation with the stress buildup. As a result, the degree to which compressive stress reduces the thermal conductivity is approximately independent of the stress value for the entire range of mismatches considered here.

(7) Two directions in which this study could be extended are as follows. The investigation of thermal stress on other diamond surfaces should enhance understanding of the dependence of the above phenomena on the surface orientation. In addition, modeling more realistic films with a columnar structure and a grain size varying in the direction of film growth[80,81] is of interest. However, the latter option could lead to considerable computational difficulties, since the typical thicknesses of such films range between 50–400 μm,[81] while the maximum sample size that we can reach with the MD simulation of diamond using the Brenner potential on a parallel 16-processor supercomputer is about 40 Å.[49]

ACKNOWLEDGMENTS

The authors would like to thank O. Glozman, A. Reznik, and S. Prawer for valuable discussions concerning experimental measurements of residual stress and swelling. The support of Israel Ministry of Science (research Grant No. 9608-2-96) in the early stages of this calculation and the support of the German Israel Foundation in the later stages are gratefully acknowledged. The calculations were carried out on the SP2 of the Inter-University Computer Center and on several computers of the Computational Physics Group and the Minerva Non-Linear Center at the Technion.

APPENDIX A: INFLUENCE OF MISMATCH AS A FUNCTION OF THE SAMPLE SIZE *L* AND THE MISMATCH FACTOR f_m

In this appendix we calculate the ‘‘influence of mismatch’’ as a function of the mismatch factor f_m and the sample size *L*. The ‘‘influence of mismatch’’ can be defined quantitatively as the average deviation from equilibrium of a bond between a diamond atom and the nearest substrate atom, $\langle \Delta r\rangle$, or, alternatively, as the degree to which the binding energy is reduced due to a mismatch, $\langle \Delta U\rangle$. For the sake of clarity, in this appendix we deal with a simple cubic lattice, and use the Morse potential[82] for carbon, with parameters $D=4.006$ eV and $\beta=1.5$ Å^{-1}.[83]

Let us consider the diamond/substrate interface with the mismatch factor f_m, previously defined [Eq. (2.1)] as the ratio of the lattice parameters of substrate (a_s) and diamond (a_d), and, obviously, equal to the ratio of the corresponding interatomic distances, l_s and l_d, in the plane parallel to the compression (the substrate is compressed, hence $l_s \leqslant l_d$ and $f_m \leqslant 1$). To illustrate our notations geometrically, in Fig. 14 we present a sample with the mismatch factor equal to $f_m = l_s/l_d = 4/5$. For the simple cubic lattice considered here the

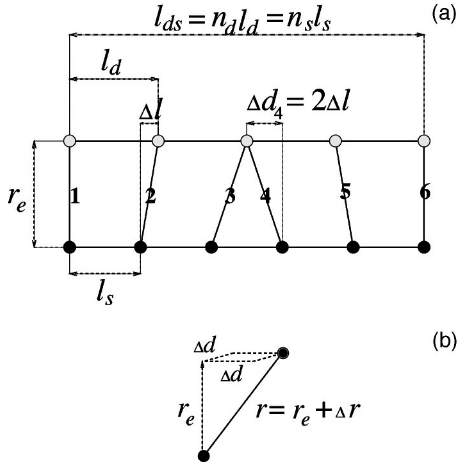

FIG. 14. Notation for Appendix A: (a) shows part of the diamond/substrate interface and (b) illustrates details of one bond. Color code: light gray—diamond atoms, black—substrate atoms.

interatomic distances in the layer are equivalent to interatomic bond lengths; we use the value of the bond length in diamond, $l_d=1.54$ Å.

We define the absolute mismatch $\Delta l \equiv l_d - l_s$ and the least common multiple of l_d and l_s, $l_{ds}\equiv n_d l_d = n_s l_s$. This is the length at which a complete substrate cell fits into a multiple of l_d (in Fig. 14 $l_{ds}=4l_d=5l_s$). The numbers of diamond (substrate) bonds in the length l_{ds} are denoted by $n_d=l_{ds}/l_d$ and $n_s=l_{ds}/l_s$, respectively; according to the definition of l_{ds}, $n_s\equiv n_d+1$ (in Fig. 14 $n_d=4$, $n_s=5$). A combination that will be used frequently below is

$$k_s\equiv n_s+1-\mathrm{mod}(n_s,2)=\begin{cases} n_s & \text{if } n_s \text{ is odd}\\ n_s+1 & \text{if } n_s \text{ is even.}\end{cases} \tag{A1}$$

The length of the whole sample (not shown in Fig. 14) is denoted by L.

Next we establish notation for differences between equilibrium and stressed configurations. If the equilibrium length of the bond between atoms in different layers (equal to the interlayer distance, 0.89 Å in case of diamond) is denoted by r_e, and the real (strained) length of this bond by r, then the deviation of the bond from equilibrium is given by $\Delta r\equiv r - r_e$. We will also refer to one-dimensional deviation of the atom starting this bond from its position in a noncompressed ideal sample, Δd. Another quantity characterizing the ''influence of mismatch'' (see above), is the per atom reduction of the binding energy of the real stressed sample compared to the nonstressed case; we denote it by ΔU.

The following additional relationships can be derived using the above definitions, in particular, that of $l_{ds}=n_d l_d = n_s l_s=(n_d+1)l_s$:

$$n_d=\frac{l_s}{l_d-l_s}=\frac{f_m l_d}{l_d-f_m l_d}=\frac{f_m}{1-f_m}, \tag{A2}$$

$$n_s=n_d+1=\frac{f_m}{1-f_m}+1=\frac{1}{1-f_m}, \tag{A3}$$

$$k_s=\frac{2-f_m}{1-f_m}-\mathrm{mod}\left(\frac{1}{1-f_m},2\right), \tag{A4}$$

$$\Delta l \equiv l_d-l_s=l_d(1-f_m)=l_s(1-f_m)/f_m. \tag{A5}$$

We start by deriving an expression for the displacement of atom starting the ith bond in the *first* period l_{ds} (in Fig. 14 only this period is shown) from its location in the absence of mismatch, Δd_i^I. For the case of n_s odd, illustrated in Fig. 14, these displacements are

$$\Delta d_1^I=0,\quad \Delta d_2^I=\Delta l,\ \ \Delta d_3^I=2\Delta l,\ \ \Delta d_4^I=2\Delta l,$$
$$\Delta d_5^I=\Delta l,\ \ \Delta d_6^I=\Delta d_1^I=0.$$

The general expression for n_s odd reads

$$\Delta d_i^I=\Delta l\left(\frac{n_s}{2}-\left|i-\frac{n_s+2}{2}\right|\right)=\begin{cases}(i-1)\Delta l & \text{for } i<(n_s+2)/2\\ (n_s+1-i)\Delta l & \text{for } i>(n_s+2)/2.\end{cases} \tag{A6}$$

Similarly, for n_s even

$$\Delta d_i^I=\Delta l\left(\frac{n_s+1}{2}-\left|i-\frac{n_s+3}{2}\right|\right)=\begin{cases}(i-1)\Delta l & \text{for } i<(n_s+3)/2\\ (n_s+2-i)\Delta l & \text{for } i>(n_s+3)/2.\end{cases} \tag{A7}$$

Applying the notation k_s, we obtain the general expression for arbitrary n_s:

$$\Delta d_i^I=\Delta l\left(\frac{k_s}{2}-\left|i-\frac{k_s+2}{2}\right|\right)=\begin{cases}(i-1)\Delta l & \text{for } i<(k_s+2)/2\\ (k_s+1-i)\Delta l & \text{for } i>(k_s+2)/2.\end{cases} \tag{A8}$$

For an *arbitrary* period l_{ds}, the displacement of an atom starting the ith bond is equal to that of its image in the *first* period:

$$\Delta d_i=\begin{cases}\Delta d^I_{\mathrm{mod}(i-1,n_s)} & \text{for } n_s \text{ odd}\\ \Delta d^I_{\mathrm{mod}(i-1,n_s+1)} & \text{for } n_s \text{ even.}\end{cases} \tag{A9}$$

Using Eq. (A8), we get the general expression for Δd_i:

$$\Delta d_i=\Delta d^I_{\mathrm{mod}(i-1,k_s)}=\Delta l\left(\frac{k_s}{2}-\left|\mathrm{mod}(i-1,k_s)-\frac{k_s+2}{2}\right|\right). \tag{A10}$$

This function is periodic in i, with the period equal to k_s.

For a sample containing N bonds the sum of all displacements, $s(N)$, is given by the series

$$s(N)=\sum_{i=1}^{N}\Delta d_i=\Delta l\sum_{i=1}^{N}\left(\frac{k_s}{2}-\left|\mathrm{mod}(i-1,k_s)-\frac{k_s+2}{2}\right|\right). \tag{A11}$$

To calculate the sum of this series, let us divide it into two parts. Assuming that the Nth bond lies in the Jth period l_{ds}, we get

$$s(N)=\sum_{j=1}^{J-1} s^j+\Delta s_N, \tag{A12}$$

where s^j is the sum over a complete period l_{ds} number j, and Δs_N is the sum over the last, incomplete period ending by the bond number N.

Considering the aforementioned periodicity, the sum over *any* complete period is equal to that over the first one, $s^j = s^I$. Hence,

$$s(N)=(J-1)s^I+\Delta s_N. \tag{A13}$$

It is easy to see that

$$s^I \equiv \sum_{i=1}^{k_s} \Delta l\left(\frac{k_s}{2}-\left|\operatorname{mod}(i-1,k_s)-\frac{k_s+2}{2}\right|\right)$$

$$=\sum_{i=1}^{\frac{k_s+1}{2}} \Delta l(i-1)+\sum_{i=\frac{k_s+3}{2}}^{k_s} \Delta l(k_s+1-i)$$

$$=\frac{\Delta l(k_s^2-1)}{8}+\frac{\Delta l(k_s^2-1)}{8}=\frac{\Delta l(k_s^2-1)}{4}. \tag{A14}$$

The number J of the period to which the last bond number N belongs is given by

$$J=[(N-1)/k_s]+1, \tag{A15}$$

and the sum over the last, Jth, incomplete period is

$$\Delta s_N=\frac{\Delta l}{8}\left(4(i'_{\text{last}}-1)i'_{\text{last}}+\left[\frac{i_{\text{last}}\cdot 2}{k_s+2}\right](4i_{\text{last}}(2k_s+1)-4i_{\text{last}}^2-1-4k_s-3k_s^2)\right), \tag{A16}$$

where $i_{\text{last}}=\operatorname{mod}(N-1,k_s)+1$ and $i'_{\text{last}}=\min[i_{\text{last}},(k_s+1)/2]$. The final expression for $s(N)$ is obtained by substituting Eqs. (A14)–(A16) into Eq. (A13).

The next step is to convert the dependence on the number of bonds $s(N)$ to that on the sample size $S(L)$. For an odd n_s the number of bonds in a sample of length L is equal to the number of atoms L/l_s+1 in the substrate layer (e.g., in Fig. 14 $n_s=5$, and the sample of length $L=l_{ds}=5l_s$ contains $l_{ds}/l_s+1=6$ bonds). If n_s is even, one additional bond builds in into each period l_{ds}, i.e., for the whole sample L/l_{ds} additional bonds build in. Therefore, the number of bonds in the sample of length L is

$$N=\begin{cases} L/l_s+1 & \text{for } n_s \text{ odd} \\ L/l_s+1+L/l_{ds}=L/l_s+1+L/(n_s l_s)=L(n_s+1)/(l_s n_s)+1 & \text{for } n_s \text{ even} \end{cases} \tag{A17}$$

and the general expression for arbitrary n_s reads

$$N\equiv Lk_s/l_s n_s+1. \tag{A18}$$

The sum of all displacements for a sample of length L is then equal to

$$S(L)=s(N)=s(Lk_s/l_s n_s+1), \tag{A19}$$

where the expression for $s(Lk_s/l_s n_s+1)$ must be taken from Eqs. (A13)–(A16).

Dividing by the number of bonds in the sample, we obtain the average displacement of a bond in the sample of length L:

$$\langle \Delta d(L,f_m)\rangle=\frac{S(L)}{N}=\frac{\Delta l(k_s^2-1)l_s n_s[L/l_s n_s]}{4(Lk_s+l_s n_s)}+\frac{\Delta s_{Lk_s/l_s n_s+1}}{Lk_s/l_s n_s+1} \tag{A20}$$

[the nonexplicit dependence on the mismatch factor f_m is inferred from the dependencies of n_s, k_s, and Δl on this parameter, Eqs. (A3)–(A5)]. The complete expression for $\Delta s_{Lk_s/l_s n_s+1}$ must be substituted from Eq. (A16).

Since the mismatch we are considering occurs in two directions (Fig. 14, lower panel), the bond length r is related to the deviations Δd by

$$r=\sqrt{r_e^2+2\Delta d^2}\approx r_e+\Delta d^2/r_e. \tag{A21}$$

The bond strain Δr is then

$$\Delta r=r-r_e\approx \Delta d^2/r_e. \tag{A22}$$

Using Eq. (A20), we obtain the average strain for the sample of length L:

$$\langle \Delta r(L,f_m)\rangle \approx \langle \Delta d(L,f_m)\rangle^2/r_e$$

$$=\frac{\Delta l^2(k_s^2-1)^2 l_s^2 n_s^2[L/l_s n_s]^2}{16 r_e(Lk_s+l_s n_s)^2}+\frac{\Delta s^2_{Lk_s/l_s n_s+1}}{r_e(Lk_s/l_s n_s+1)^2}. \tag{A23}$$

Again, the dependence on the mismatch factor f_m is inferred from the dependencies of n_s, k_s, and Δl on this parameter [Eqs. (A3), (A4), and (A5)], and the complete expression for $\Delta s_{Lk_s/l_s n_s+1}$ can be substituted from Eq. (A16).

The derived dependence of $\langle \Delta r\rangle$ on sample size L and on mismatch factor f_m, Eq. (A23), is plotted in Fig. 3(a). The behavior of this quantity appears to be highly oscillatory at small L [$\sim l_{ds}=l_d f_m/(1-f_m)$] and saturates to a limit at $L \to \infty$ (see below). A qualitative explanation of such dependence is given in the main text (Sec. II B).

The obtained mismatch-induced deviation from equilibrium of the bond length can be used to estimate the binding-energy reduction caused by mismatch. For a rough estimation some simple pairwise interaction potential, like that of Morse,[82] $U_{\text{bond}}(\Delta r)=D[1-\exp(-\beta\Delta r)]^2$, can be assumed. Considering that in diamond there are two bonds per atom (each atom is connected by four bonds, and each bond is shared by two atoms), the reduction of the binding energy per atom can be estimated to be

$$\begin{aligned}\Delta U(\Delta r)&=2[U_{\text{bond}}(0)-U_{\text{bond}}(\Delta r)]\\&=2D[-1-\exp(-2\beta\Delta r)\\&\quad+2\exp(-\beta\Delta r)].\end{aligned}\tag{A24}$$

Averaging over bonds with various strains (i.e., substituting $\langle\Delta r\rangle$ instead of Δr), we get the average weakening of the binding energy of the sample of size L due to mismatch f_m:

$$\begin{aligned}\langle\Delta U(L,f_m)\rangle&=2D\{-1-\exp[-2\beta\langle\Delta r(L,f_m)\rangle]\\&\quad+2\exp[-\beta\langle\Delta r(L,f_m)\rangle]\},\end{aligned}\tag{A25}$$

where the expression for $\langle\Delta r(L,f_m)\rangle$ must be taken from Eq. (A23).

The function Eq. (A25) is plotted in Fig. 3(b). Again, the behavior is oscillatory at small L and saturates to a limit at $L\rightarrow\infty$. This means that for large enough samples the reduction of the binding energy is independent of L, and only a (rather weak and nonmonotonous) dependence on f_m remains. A qualitative explanation of such behavior is given in the main text (Sec. II B).

As shown above, for large sample sizes L the quantities $\langle\Delta r(L,f_m)\rangle$ and $\langle\Delta U(L,f_m)\rangle$ converge to some asymptotic values. Let us find these "saturation limits." Using Eq. (A20), we find the limit of $\langle\Delta d(L,f_m)\rangle$ to be

$$\begin{aligned}\langle\Delta d_\infty(f_m)\rangle&=\lim_{L\rightarrow\infty}\langle\Delta d(L,f_m)\rangle\\&\equiv\lim_{L\rightarrow\infty}\frac{\Delta l(k_s^2-1)l_sn_s[L/l_sn_s]}{4(Lk_s+l_sn_s)},\end{aligned}\tag{A26}$$

since

$$\frac{\Delta s_{Lk_s/l_sn_s+1}}{Lk_s/l_sn_s+1}\rightarrow 0$$

at $L\rightarrow\infty$. Considering that

$$\lim_{L\rightarrow\infty}\frac{l_sn_s[L/l_sn_s]}{Lk_s+l_sn_s}=\frac{1}{k_s}\tag{A27}$$

and substituting expressions Eqs. (A3)–(A5) for n_s, k_s, and Δl, we get

$$\langle\Delta d_\infty(f_m)\rangle=\begin{cases}\dfrac{l_df_m(2-f_m)}{4} & \text{for } n_s=1/(1-f_m) \text{ odd}\\[2ex] \dfrac{l_d(3-2f_m)}{4(2-f_m)} & \text{for } n_s=1/(1-f_m) \text{ even,}\end{cases}\tag{A28}$$

or, expressing this by one equation,

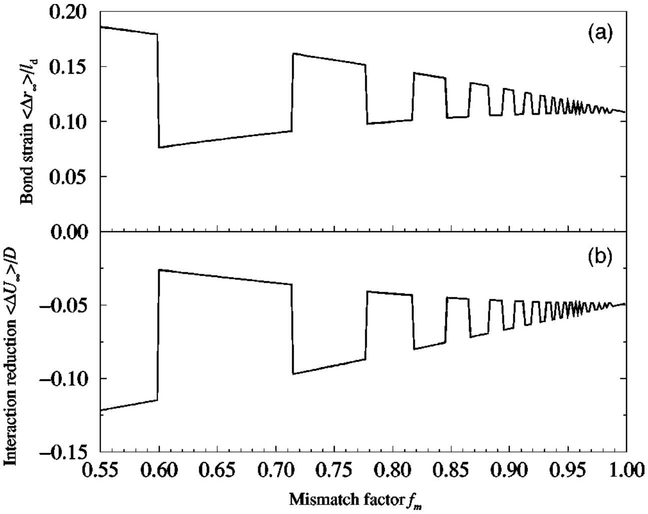

FIG. 15. Large-sample limits (a) of the average bond strain (in units of the diamond bond length, $l_d=1.54$ Å) and (b) of the reduction of the binding energy per atom (in units of the well depth D); drawn according to Eqs. (A31) and (A32).

$$\begin{aligned}\langle\Delta d_\infty(f_m)\rangle&=\text{mod}[1/(1-f_m),2]l_d\frac{f_m(2-f_m)}{4}\\&\quad+\text{mod}[1/(1-f_m)+1,2]l_d\frac{3-2f_m}{4(2-f_m)}.\end{aligned}\tag{A29}$$

Two features of this result should be noted. First, the dependence of the saturation limit on f_m is nonmonotonic: for an odd n_s it grows with f_m, while for an even n_s it decreases. In reality, n_s does not have to be an integer, and, although the general tendency for $\langle\Delta d_\infty\rangle$ is to decrease with f_m, the dependence still remains nonmonotonic. Second, for f_m close to 1 (as it is in reality), for both n_s either odd or even

$$\langle\Delta d_{\infty,f_m\sim 1}\rangle\approx l_d/4.\tag{A30}$$

Using the relationships (A23) and (A25), we finally obtain

$$\langle\Delta r_\infty(f_m)\rangle\approx\langle\Delta d_\infty(f_m)\rangle^2/r_e,\tag{A31}$$

$$\begin{aligned}\langle\Delta U_\infty(f_m)\rangle&\approx 2D\{-1-\exp[-2\beta\langle\Delta r_\infty(f_m)\rangle]\\&\quad+2\exp[-\beta\langle\Delta r_\infty(f_m)\rangle]\}.\end{aligned}\tag{A32}$$

These functions are plotted in Fig. 15, where we observe that, in accordance with Eq. (A30), for a realistic value of f_m close to unity, these limits are

$$\langle\Delta r_{\infty,f_m\sim 1}\rangle\approx l_d^2/16r_e,\tag{A33}$$

$$\begin{aligned}\langle\Delta U_{\infty,f_m\sim 1}\rangle&\approx 2D[-1-\exp(-2\beta l_d^2/16r_e)\\&\quad+2\exp(-\beta l_d^2/16r_e)],\end{aligned}\tag{A34}$$

or, using the numeric values of parameters given above,

$$\langle \Delta r_{\infty, f_m \sim 1} \rangle \approx 0.108 \ \ l_d, \tag{A35}$$

$$\langle \Delta U_{\infty,\ f_m \sim 1} \rangle \approx -0.1D$$

$$(10\% \ \ \text{weakening of the interaction}). \tag{A36}$$

Summarizing, we can note that, though all above estimations are rough (containing many approximations and not considering the specific structure of the lattice), they still allow us to understand how the ''influence of mismatch'' depends on sample size L and on mismatch factor f_m (Fig. 3): for small samples $[L \sim l_{ds} = l_d f_m/(1-f_m)]$ it is highly sensitive to both sample size and mismatch factor, while for large samples only the dependence on f_m remains [Eqs. (A31) and (A32)].

Moreover, for large samples, if the mismatch factor is close to 1 (as it is in reality), also this last dependence is almost eliminated: for all values of f_m the influence of mismatch is nearly the same and corresponds to approximately a 10% weakening of the interaction [Eqs. (A33)–(A36)].

Finally, the period necessary to achieve the ''saturation limit'' at which the influence of mismatch becomes insensitive to the sample size depends on the value of mismatch factor: the smaller f_m (i.e., the larger the mismatch), the sooner (for smaller L) this ''saturation limit'' is achieved (Fig. 3).

APPENDIX B: EVALUATION OF RAYLEIGH COEFFICIENTS FOR THREE DEFECTS: GRAPHITELIKE CARBON ATOM IN sp^2 CONFIGURATION, TETRAHEDRAL AMORPHOUS CARBON *ta*-C, AND ⟨100⟩ SPLIT INTERSTITIAL

According to Ref. 84, the Rayleigh coefficient I for the scattering on point defects is given by

$$I = \frac{ca^3k^4}{4\pi v^3\hbar^4}\left(\frac{\Delta M}{M} + 2\gamma p\right)^2, \tag{B1}$$

where c is the concentration of defects, a^3 is the volume per atom (for diamond equal to 5.67×10^{-24} cm^3/atom at RT), v is the velocity of sound in the material, 1.195×10^6 cm/s,[26] ΔM is the mass change due to replacement of the parent atom of mass M by the defect atom of mass $M+\Delta M$, γ is the Grüneisen parameter (equal to 1.1 for diamond[85]), and p is the fractional volume difference accounted due to the defect.

In our simulation all defects are local inhomogeneities and have the same mass as the parent atoms. Hence, the point defect scattering is due only to the difference in the volume occupied by an ideal diamond atom and that of a defect. Therefore, Eq. (B1) simplifies to

$$I = \frac{ca^3k^4}{4\pi v^3\hbar^4}(2\gamma p)^2, \tag{B2}$$

and the only defect-specific quantity that remains to be calculated is the fractional volume difference p of each particular defect:

$$p \equiv \frac{v_{\mathrm{p.d.}} - v_{\mathrm{d}}}{v_{\mathrm{d}}}, \tag{B3}$$

where $v_{\mathrm{p.d.}}$ and v_{d} are the atomic volume of point defect and of ideal diamond, correspondingly.

Let us now estimate the values of p and I for the three defects relevant to the present study, namely, for the graphitelike carbon atom in sp^2 configuration, for the tetrahedral amorphous carbon *ta*-C, and for the ⟨100⟩ split interstitial.

First we consider the isolated graphitelike three-fold carbon atom in the sp^2 configuration. The configuration of this defect is equivalent to that of a carbon atom in graphite. Therefore, its atomic volume v_{sp^2} is equal to the atomic volume v_{g} of graphite, and the fractional volume difference for this defect p_{sp^2} is given by

$$p_{sp^2} \equiv \frac{v_{sp^2} - v_{\mathrm{d}}}{v_{\mathrm{d}}} \approx \frac{v_{\mathrm{g}} - v_{\mathrm{d}}}{v_{\mathrm{d}}}, \tag{B4}$$

where the subscript ''sp^2'' stands for the ''isolated graphitelike three-fold carbon defect in the sp^2 configuration.'' With the values $v_{\mathrm{d}} = 5.65\times10^{-24}$ cm^3/atom and $v_{\mathrm{g}} = 8.77\times10^{-24}$ cm^3/atom,[67] p_{sp^2} and, consequently, I_{sp^2} take the values

$$p_{sp^2} \approx 0.552, \quad I_{sp^2} \approx 114.48c \ \mathrm{K}^{-4}\,\mathrm{s}^{-1}, \tag{B5}$$

c being the dimensionless atomic concentration of defects in question.

Next, we estimate the values of p and I for the intermediate tetrahedral amorphous carbon defect *ta*-C. The configuration of this defect is intermediate between graphite and diamond; according to Refs. 30 and 38, its coordination number is equal to 3.7. This means that this defect can be considered to be 70% diamondlike and 30% graphitelike in character, and its atomic volume to be approximately equal to

$$v_{ta\text{-C}} \approx 0.7v_{\mathrm{d}} + 0.3v_{\mathrm{g}}. \tag{B6}$$

This gives the fractional volume difference of

$$p_{ta\text{-C}} \equiv \frac{v_{ta\text{-C}} - v_{\mathrm{d}}}{v_{\mathrm{d}}} \approx \frac{0.3(v_{\mathrm{g}} - v_{\mathrm{d}})}{v_{\mathrm{d}}}. \tag{B7}$$

For the above values of v_{d} and v_{g} this volume difference and the corresponding Rayleigh coefficient $I_{ta\text{-C}}$ take the values

$$p_{ta\text{-C}} \approx 0.166, \quad I_{ta\text{-C}} \approx 9.84c \ \mathrm{K}^{-4}\,\mathrm{s}^{-1}, \tag{B8}$$

where c is the atomic concentration of *ta*-C defects.

Finally, we consider the ⟨100⟩ split interstitial. It would seem reasonable to determine the effective volume of a split interstitial v_{si} from the experiments on diamond implantation, provided that (1) it is known that the produced defects are split interstitials, (2) their concentration is known, and (3) the swelling of the diamond lattice due to these defects is known (e.g., from the step height measurements[86]).

This approach, however, is subject to two main difficulties. First, the standard Monte Carlo computer code TRIM used for the calculation of defects concentration in implantation experiments completely ignores dynamic annealing that repairs the lattice almost instantaneously;[87] hence, the concentration of defects given by TRIM is highly overestimated (sometimes, by several orders).[88] Second, in experiment it is impossible to obtain only one sort of defects: the implantation always results in the formation of both vacancies and split interstitials, as well as of the partially graphitized regions.[88,89] To overcome these difficulties, high-energy implantation experiments in which a single vacancy-interstitial pair will be created in one ion hit[87] are desirable; however, to the best of our knowledge, such experiments on diamond have not been done yet.

Thus, since appropriate experimental data are lacking, we estimate the volume expansion of diamond due to a $\langle 100 \rangle$ split interstitial from simulation results. In Ref. 26 a dumbbell was created at a separation of 1.27 Å, i.e., one $\langle 100 \rangle$ split interstitial was artificially inserted into the *nonexpanded* diamond lattice. This defect was annealed, and the dumbbell separation relaxed to 1.47 Å. Considering that the dumbbell defect is linear, the ratio of these quantities, 1.47/1.27, may serve as a rough estimation of the extent to which a single $\langle 100 \rangle$ split interstitial expands the surrounding diamond lattice:

$$v_{\mathrm{si}}/v_{\mathrm{d}} \approx 1.47/1.27. \tag{B9}$$

With this estimation the fractional volume difference due to $\langle 100 \rangle$ split interstitial p_{si} and the corresponding Rayleigh coefficient I_{si} take the values

$$p_{\mathrm{si}} \equiv \frac{v_{\mathrm{si}} - v_{\mathrm{d}}}{v_{\mathrm{d}}} = \frac{v_{\mathrm{si}}}{v_{\mathrm{d}}} - 1 \approx 1.47/1.27 - 1 = 0.157,$$

$$I_{\mathrm{si}} \approx 9.31c\ \mathrm{K}^{-4}\,\mathrm{s}^{-1}. \tag{B10}$$

Comparison between the fractional volume expansion due to an isolated sp^2-configurated three-fold atom, $p_{sp^2} \approx 0.552$, to an ‘‘intermediate’’ *ta*-C defect, $p_{ta\text{-}\mathrm{C}} \approx 0.166$, and to a $\langle 100 \rangle$ split interstitial, $p_{3\mathrm{i}} \approx 0.157$, demonstrates that the former defect is much less compact than the others and hence is expected to be consistent with lower values of pressure (stress). The most compact defect is the $\langle 100 \rangle$ split interstitial; it is likely to form when the volume is most restricted, e.g., for a high degree of the film continuity.

---

*Corresponding author. Fax: 972-4-8221514. E-mail: phr76ja@phjoan.technion.ac.il

[1] M. Seal, Interdisc. Sci. Rev. **14**, 64 (1989).

[2] Y. Sato and M. Kamo, in *The Properties of Natural and Synthetic Diamond*, edited by J.E. Field (Academic, New York, 1992), p. 42.

[3] J.E. Graebner, in *Diamond: Electronic Properties and Applications*, edited by L.S. Pan and D.R. Kania (Kluwer Academic, Dodrecht, 1995), p. 285.

[4] C.P. Klages, Appl. Phys. A: Solids Surf. **56**, 53 (1993).

[5] W. Zhu, B.R. Stoner, B.E. Williams, and J.T. Glass, Proc. IEEE **79**, 621 (1991).

[6] W.A. Yarbrough and R. Messier, Science **24**, 688 (1990).

[7] O. Glozman and A. Hoffman, Diamond Relat. Mater. **6**, 796 (1997).

[8] O. Glozman and A. Hoffman, Diamond Relat. Mater. **6**, 1847 (1997).

[9] H. Windischmann, G.F. Epps, Y. Cong, and R.W. Collins, J. Appl. Phys. **69**, 2231 (1991).

[10] H. Windischmann and K.J. Gray, Diamond Relat. Mater. **4**, 837 (1995).

[11] K.H. Chen, Y.L. Lai, J.C. Lin, K.J. Song, L.C. Chen, and C.Y. Huang, Diamond Relat. Mater. **4**, 460 (1995).

[12] S.A. Stuart, S. Prawer, and P.S. Weiser, Appl. Phys. Lett. **62**, 1227 (1993).

[13] S. Haq, D.L. Tunnicliff, S. Sails, and J. Savage, Appl. Phys. Lett. **68**, 469 (1996).

[14] L.J. Bernardez and K.F. McCart, Diamond Relat. Mater. **3**, 22 (1993).

[15] J.A. Baglio, B.C. Farnsworth, S. Hankin, S. Hamill, and D. O’Neil, Thin Solid Films **212**, 180 (1992).

[16] A. Fayer, O. Glozman, and A. Hoffman, Appl. Phys. Lett. **67**, 2299 (1995).

[17] C. Kittel, *Introduction to Solid State Physics*, 2nd ed. (Wiley, New York, 1960).

[18] A.K. Ramdas, EMIS Datarev. Ser. **9**, 13 (1993).

[19] J.W. Ager III, and M. Drory, Phys. Rev. B **48**, 2601 (1993).

[20] D.S. Knight and W.B. White, J. Mater. Res. **3**, 1043 (1988).

[21] M. Yoshikawa, H. Ishida, A. Ishitani, T. Murakami, S. Koizumi, and T. Inuzuka, Appl. Phys. Lett. **57**, 428 (1990).

[22] W. Wanlu, L. Kejun, G. Jinying, and L. Aimin, Thin Solid Films **215**, 174 (1992).

[23] M.H. Grimsditch, E. Anastassakis, and M. Cardona, Phys. Rev. B **18**, 901 (1978).

[24] O. Glozman, Ph.D. thesis, Technion, Israel Institute of Technology, 1998.

[25] C.H. Li, *Metal-Ceramic Joining Symposium*, TMC Fall Meeting (Minerals, Metals and Materials Society, Warrendale, 1991).

[26] I. Rosenblum, J. Adler, and S. Brandon, Comput. Mater. Sci. **12**, 9 (1998).

[27] Y. Uemura, Phys. Rev. B **49**, 6528 (1994).

[28] Y. Uemura, Phys. Rev. B **51**, 6704 (1995).

[29] B.A. Pailthorpe, J. Appl. Phys. **70**, 543 (1991).

[30] D.R. McKenzie, D. Muller, and B.A. Pailthorpe, Phys. Rev. Lett. **67**, 773 (1991).

[31] B.A. Pailthorpe, D. Mitchell, and N.S. Bordes, Thin Solid Films **332**, 109 (1998).

[32] B.A. Pailthorpe and P. Knight, in *Low Energy Ion Beam and Plasma Modification of Materials Symposium* (Material Research Society, Pittsburgh, 1991), p. 29.

[33] B.A. Pailthorpe and P. Mahon, Thin Solid Films **193**, 34 (1990).

[34] E.G. Gerstner and B.A. Pailthorpe, J. Non-Cryst. Solids **189**, 258 (1995).

[35] N.A. Marks, P. Guan, D.R. McKenzie, and B.A. Pailthorpe, in *Mechanisms of Thin Film Evolution Symposium* (Material Research Society, Pittsburgh, 1994), p. 497.

[36] N.A. Marks, D.R. McKenzie, and B.A. Pailthorpe, J. Phys.: Condens. Matter **6**, 7833 (1994).

[37] D.R. McKenzie, N.A. Marks, P. Guan, B.A. Pailthorpe, W.D. McFall, and Y. Yin, in *Surface Science. Principles and Current Applications* (Springer-Verlag, Berlin, 1996), p. 250.

[38] D.R. McKenzie, D. Muller, B.A. Pailthorpe, Z.H. Wang, E. Kravtchinskaia, D. Segal, P.B. Lukins, P.D. Swift, P.J. Martin, G. Amaratunga, P.H. Gaskell, and A. Saeed, Diamond Relat. Mater. **1**, 51 (1991).

[39] D.W. Brenner, Phys. Rev. B **42**, 9458 (1990).

[40] M. Parrinello and A. Rahman, Phys. Rev. Lett. **45**, 1196 (1980).

[41] M. Parrinello and A. Rahman, J. Appl. Phys. **52**, 7182 (1981).

[42] J.R. Ray and A. Rahman, J. Chem. Phys. **80**, 4423 (1984).

[43] J.R. Ray and A. Rahman, J. Chem. Phys. **82**, 4243 (1985).

[44] M.W. Ribarsky and U. Landman, Phys. Rev. B **38**, 9522 (1988).

[45] Z.-G. Wang, U. Landman, R.L. Blumberg-Selenger, and W.M. Gelbert, Phys. Rev. B **44**, 378 (1991).

[46] Note that implicit in this definition is the assumption that α is isotropic.

[47] C. Zuiker, A.R. Krauss, D.M. Gruen, X. Pan, J.C. Li, R. Csencsits, A. Erdemir, S. Bindal, and G. Fenske, Thin Solid Films **270**, 154 (1995).

[48] G.A. Slack and S.F. Bartram, J. Appl. Phys. **46**, 89 (1975).

[49] I. Rosenblum, J. Adler, and S. Brandon, Int. J. Mod. Phys. C **10**, 189 (1999).

[50] M.P. Allen and D.J. Tildesley, *Computer Simulation of Liquids* (Clarendon, Oxford, 1994).

[51] D.C. Rapaport, *The Art of Molecular Dynamics Simulation* (University Press, Cambridge, 1995).

[52] Use of the ''edge rescaling'' method (Refs. 26 and 90) is undesirable since it could introduce some artificial ''substrate'' effects, and the introduction of the random phase into the velocity rescaling procedure (Ref. 29) or using one of the constraint methods of the temperature maintenance (Refs. 50 and 91) would considerably disturb the velocity-velocity autocorrelation function that we need for the determination of the phonon spectra.

[53] *Handbook of Physics*, edited by E.U. Condon and H. Odishaw (McGraw-Hill, New York, 1958).

[54] M.H. Grimsditch and A.K. Ramdas, Phys. Rev. B **11**, 3139 (1975).

[55] S. Sengupta, P. Nielaba, M. Rao and K. Binder, Johannes Gutenberg Universität Mainz, preprint, 1999.

[56] J.E. Field, *The Properties of Diamond* (Academic, London, 1979).

[57] K. Kendall, Nature (London) **272**, 710 (1978).

[58] F.C. Roesler, Proc. Phys. Soc. **69**, 55 (1956).

[59] D. Saada, J. Adler, and R. Kalish, Phys. Rev. B **59**, 6650 (1999).

[60] E. Gheeraert, A. Deneuville, A.M. Bonnot, and L. Abello, Diamond Relat. Mater. **1**, 525 (1992).

[61] M. Lannoo and J. Bourgoin, *Point Defects in Semiconductors, Vols. I and II. Theoretical Aspects* (Springer-Verlag, Berlin, 1981).

[62] C.Z. Wang and K.M. Ho, Phys. Rev. Lett. **71**, 1184 (1993).

[63] If determined straightforwardly, i.e., by calculating the number of the nearest neighbors located inside some preset cutoff radius r_c.

[64] P.J. Lin-Chung, Phys. Rev. B **50**, 16 905 (1994).

[65] S. Prawer, J. Orwa, I. Rosenblum, and J. Adler (unpublished).

[66] J. Orwa (private communications).

[67] M.S. Dresselhaus and R. Kalish, *Implantation in Diamond, Graphite and Related Materials* (Springer-Verlag, Berlin, 1992).

[68] The activation energy for the $sp^3 \rightarrow sp^2$ conversion was recently estimated to be about 0.7 eV (Ref. 92); this energy is acquired from the stress-induced binding energy reduction (Fig. 5) and from the local temperature fluctuations.

[69] *Physical Properties of Diamond*, edited by R. Berman (Clarendon, Oxford, 1965).

[70] Swelling is usually observed in implantation experiments, where it results either from a partial diamond graphitization caused by ion irradiation (Ref. 71) or from the diffusion of various irradiation-induced defects (Refs. 72 and 89).

[71] E.W. Maby, C.W. Magee, and J.H. Morewood, Appl. Phys. Lett. **39**, 157 (1981).

[72] J.F. Prins, T.E. Derry, and J.P.F. Sellschop, Phys. Rev. B **34**, 8870 (1986).

[73] D. Saada, J. Adler, and R. Kalish, Int. J. Mod. Phys. C **9**, 61 (1998).

[74] S.J. Breuer and P.R. Briddon, Phys. Rev. B **51**, 6984 (1994).

[75] J. Bernholc, A. Antonelli, T.M. Del Sol, Y. Bar-Yam, and S.T. Pantelides, Phys. Rev. Lett. **61**, 2689 (1988).

[76] At the highest film continuity, when the stress builds up, the increase of the concentration of all defects (in particular, of ''amorphous carbon'') prevails over the conversion of ''amorphous carbons'' to split interstitials, and the intensity of the amorphous carbon peak starts growing again; in experiment this stage is, apparently, not achieved.

[77] K. Belay, Z. Etzel, D.G. Onn, and T.R. Anthony, J. Appl. Phys. **79**, 8336 (1996).

[78] J.E. Graebner, J.A. Mucha, and F.A. Baiocchi, Diamond Relat. Mater. **5**, 682 (1996).

[79] J.T. Houghton and S.D. Smith, *Infra-Red Physics* (Clarendon, Oxford, 1966).

[80] J.E. Graebner, S. Jin, G.W. Kamlott, J.A. Herb, and C.F. Gardinier, Appl. Phys. Lett. **60**, 1576 (1992).

[81] J.E. Graebner, S. Jin, G.W. Kammlott, Y.-H. Wong, A. Herb, and C.F. Gardinier, Diamond Relat. Mater. **2**, 1059 (1993).

[82] W.J. Moore, *Physical Chemistry* (Longmans, London, 1961).

[83] P. Jensen, C.M. Rohlfing, and J. Almlöf, J. Chem. Phys. **97**, 3399 (1992).

[84] L.A. Turk and P.G. Klemens, Phys. Rev. B **9**, 4422 (1974).

[85] R. Berman, P.R.W. Hudson, and M. Martinez, J. Phys. C: Solid State Phys. (UK) **8**, L430 (1975).

[86] S. Prawer, A. Hoffman, and R. Kalish, Appl. Phys. Lett. **57**, 2187 (1990).

[87] S. Prawer (private communications).

[88] S. Prawer and R. Kalish, Phys. Rev. B **51**, 15 711 (1995).

[89] R. Kalish, A. Reznik, K.W. Nugent, and S. Prawer, Nucl. Instruction Methods Phys. Res. B (to be published).

[90] H.C. Berendsen, J.P.M. Postma, W.F. van Gunsteren, A. DiNola, and J.R. Haak, J. Chem. Phys. **81**, 3684 (1984).

[91] D.J. Evans and G.P. Morris, Comput. Phys. Rep. **1**, 297 (1984).

[92] A. Reznik, V. Richter, and R. Kalish, Phys. Rev. B **56**, 7930 (1997).